Title

Global metabolic profiles in a non-human primate model of maternal immune activation: implications for neurodevelopmental disorders

Journal

Molecular Psychiatry, 27(12)

ISSN

1359-4184

Authors

Boktor, Joseph C

Adame, Mark D

Rose, Destanie R

et al.

Publication Date

2022-12-01

DOI

10.1038/s41380-022-01752-y

Peer reviewed

HHS Public Access

Author manuscript

Mol Psychiatry. Author manuscript; available in PMC 2023 June 01.

Published in final edited form as:

Mol Psychiatry. 2022 December ; 27(12): 4959–4973. doi:10.1038/s41380-022-01752-y.

Global Metabolic Profiles in a Non-human Primate model of Maternal Immune Activation: implications for neurodevelopmental disorders

Joseph C. Boktor[1], **Mark D. Adame**[1], **Destanie R. Rose**[2,3], **Cynthia M. Schumann**[3], **Karl D. Murray**[3], **Melissa D. Bauman**[3], **Milo Careaga**[2,3], **Sarkis K. Mazmanian**[1], **Paul Ashwood**[2,3,†], **Brittany D. Needham**[4,†]

[1]Biology and Biological Engineering, California Institute of Technology, Pasadena, CA, 91125, USA

[2]Department of Medical Microbiology and Immunology, University of California Davis, Davis, CA, 95616, USA

[3]The M.I.N.D. Institute, University of California, Davis, Sacramento, CA, 95817, USA

[4]Department of Anatomy, Cell Biology & Physiology, Stark Neurosciences Research Institute, Indiana University School of Medicine, Indianapolis, IN, 46202, USA

Abstract

Epidemiological evidence implicates severe maternal infections as risk factors for neurodevelopmental disorders, such as ASD and schizophrenia. Accordingly, animal models mimicking infection during pregnancy, including the maternal immune activation (MIA) model, result in offspring with neurobiological, behavioral, and metabolic phenotypes relevant to human neurodevelopmental disorders. Most of these studies have been performed in rodents. We sought to better understand the molecular signatures characterizing the MIA model in an organism more closely related to humans, rhesus monkeys (*Macaca mulatta*), by evaluating changes in global metabolic profiles in MIA-exposed offspring. Herein, we present the global metabolome in six peripheral tissues (plasma, cerebrospinal fluid, three regions of intestinal mucosa scrapings, and feces) from 13 MIA and 10 control offspring that were confirmed to display atypical neurodevelopment, elevated immune profiles, and neuropathology. Differences in lipid, amino acid, and nucleotide metabolism discriminated these MIA and control samples, with correlations of specific metabolites to behavior scores as well as to cytokine levels in plasma, intestinal, and brain tissues. We also observed modest changes in fecal and intestinal microbial profiles, and identify differential metabolomic profiles within males and females. These findings support a connection between maternal immune activation and the metabolism, microbiota, and behavioral

[†]Corresponding authors: Correspondence: needham@iu.edu, and pashwood@ucdavis.edu.

Author contributions: M.D.B., C.M.S., K.D.M., and M.C..worked directly with the NHPs and collected samples. D.R.R. performed immune profiling. J.C.B., M.D.A., and B.D.N. analyzed metabolomics data and wrote the manuscript. S.K.M, P.A. and M.D.B. secured funding for the project. All authors edited the manuscript.

Declaration of Interests

S.K.M. has financial interest in Axial Biotherapeutics. J.C.B., M.D.A., D.R.R., C.M.S., K.D.M., M.D.B., M.C., P.A., and B.D.N. report no financial conflicts of interest.

traits of offspring, and may further the translational applications of the MIA model and the advancement of biomarkers for neurodevelopmental disorders such as ASD or schizophrenia.

Keywords

Autism Spectrum Disorder; ASD; Non-human primates; metabolomics; plasma; cerebrospinal fluid; intestinal mucosal scrapings; fecal samples

INTRODUCTION

Behavioral manifestations, including impaired social communication and restricted repetitive behavior, are the sole criteria for diagnosis of neurodevelopmental disorders (NDD) such as ASD or schizophrenia, impeding early detection for immediate behavioral therapy intervention[1, 2]. Recent advances in untargeted global metabolome characterization offer the potential for discovery of biomarkers and disease-relevant alterations in metabolism. Although ASD is highly heritable with hundreds of known genetic risk factors, gene-environment interactions appear to play a critical role[3, 4], with indication that factors such as prenatal conditions[5] , exposure to toxins or certain pharmaceuticals[6–8], and alterations in intestinal microbial communities could be involved[9–15].

The diversity of prenatal infectious agents associated with increased risk of NDD suggests that activation of the maternal immune system is the key link between maternal infections and altered fetal brain development. This MIA hypothesis has been tested in animal model systems by activating the immune system during pregnancy and quantifying changes in offspring brain and behavioral development that parallel features of human NDDs[16]. When pregnant mice are exposed to infection, or microbial components mimicking infection, offspring show behavioral alterations consistent with the core features of NDDs[10, 16, 16–19]. These effects are driven by the cytokines IL-6 and IL-17[10, 20–22] and appear to be regulated at least in part by gut microbial influence[10, 23]. In recent years, the MIA model has evolved from the initial characterization as model of ASD or SZ towards a more hypothesis-based model for examining the effects of maternal inflammation on neural systems relevant to multiple neurodevelopmental conditions[24]. MIA offspring display neurological phenotypes characterized by key changes at the level of transcription, cellular morphology and quantity, neural signaling, and regional development[17, 18, 25–29].

To better approximate the behavioral and biochemical features of human NDDs, nonhuman primate (NHP) models of MIA have been developed[30]. MIA offspring in the NHP model display altered social communication and increased stereotypy, evidenced through abnormal social attention and interaction[31, 32], altered responses in infancy and weaning tests[31, 33], and increased repetitive behaviors[31]. Further studies have corroborated long-lasting immune dysregulation in MIA offspring, including increased innate immune responses that correlated with some behavioral phenotypes[34], as well as neurobiological phenotypes such as altered volume of white and grey matter[33, 35, 36], neurotransmitter levels[37], neuronal morphology[38] and region specific gene expression[39, 40].

In humans, various metabolic changes have been observed between ASD and typically developing individuals that may prove useful as biomarkers or therapeutic targets. A panel based on three categories of metabolites represented by sarcosine, inosine 5-monophosphate, and tyramine O-sulfate showed high predictive power for ASD classification[41]. Amino acid metabolism is also often implicated in ASD[42–49], and certain ratios of branched amino acids have even shown potential to discriminate between blood samples of ASD and typically developing individuals[50]. Along with this, aromatic and phenolic metabolites may be differentially excreted in urine in ASD individuals, including derivatives of nicotinic, amino acid, and hippurate metabolism[46, 49, 51–55]. Further, levels of lipids, such as acyl-carnitines, plasmalogens, short chain fatty acids, and poly-unsaturated fatty acids, appear to be altered[48, 56–63]. Interestingly, in various studies of ASD plasma samples, indicators of oxidative stress, cellular energy and mitochondrial dysfunction have been found[64–69]. Taken together these results suggest that metabolic profiles of ASD individuals display distinct signatures that provide insight into disease pathology.

Metabolic changes have also been studied in MIA rodents, with one broad study revealing alterations in the levels of 8% of serum metabolites[10]. Amino acid and lipid pathways displayed robust signatures, including tryptophan and tyrosine metabolites, which were restored along with behavioral deficits by a probiotic bacterial treatment[10]. Purinergic metabolites have also been observed at altered levels in MIA mice, and an antipurinic therapeutic restored normal metabolism and behavior[70]. Thus far, similar studies have not been performed on NHP MIA models. Bridging the gap between mouse models of MIA and human ASD may enable mechanistic discoveries of pathology and novel treatments for ASD targeting specific metabolic pathways or microbial influences.

METHODS AND MATERIALS

All experiments were approved by the University of California, Davis Institutional Animal Care and Use Committee. Study design and experimental methods used in this study were developed in consultation with the California National Primate Research Center veterinary staff. To promote the psychological well-being of study animals, all attempts were made to ensure animals had social housing, an enriched diet, use of positive reinforcement strategies, and minimal training/testing sessions. Detailed methods on the administration of polyinosinic:polycytidylic acid stabilized with poly-L-lysine (poly ICLC), rearing conditions and behavioral observations have been previously published[35,38] and are described in brief below.

Maternal Administration of Poly ICLC

24 pregnant rhesus monkeys were placed into two main treatment groups, controls or MIA, and each dam gave birth to a single infant. Our NHP poly ICLC-based MIA model is designed to stimulate inflammatory cytokine response late in the first trimester that mimics a moderate to severe infection during pregnancy. MIA induction protocols are based on our previous dosing and gestational timing experiments previously described[31, 32, 37, 38]. For animals that received poly ICLC, three injections of 0.25 mg/kg of poly ICLC (Oncovir, Inc., Washington, DC) were administered intravenously either in the first trimester or the

second trimester (typical gestation length of rhesus macaques is approximately 165 days). First trimester injections of either poly ICLC or saline were administered to the dams at 8 am on gestational days 43, 44, and 46 and included a total of 10 dams (poly ICLC, n=6; saline, n=4). Second trimester dams were injected at 8 am on gestational days 100, 101 and 103. For a final total available for this study being first semester (n=6) or second trimester (n=7). A total of 11 dams received injections during the second trimester (poly IC, n=7; saline, n=4). Three untreated (no administration of saline or poly ICLC) animals were also included to determine whether there was an effect of saline on behavioral and immune outcomes. Previous characterization of the NHPs in this study also revealed no distinctions between saline and untreated controls, and only minor differences associated with timing of poly ICLC injection; thus the two control groups and two MIA groups, respectively, were merged for this study. Three control animals were not euthanized and only plasma was collected (n=8 for saline group in CSF, intestinal scrapings, feces), with one plasma sample lost due to thawing (n=10 for saline group in plasma).

Rearing conditions

Mother and infant pairs were housed in individual cages with continual visual access to other animals. All mother-infant pairs participated in social groups of 4 mother-infant dyads plus an adult male. Groups of four mother-infant pairs and an adult male were placed in large chain link enclosures for three hours a day to encourage species-typical social development and for social enrichment. Each of these socialization groups were randomized and were comprised of both control and treatment males and females. These groups were maintained from birth until weaning at 6 months of age. Weanlings continued daily group socialization sessions with the same four offspring, the adult male, plus an adult female from 6 months of age through approximately 2 years of age. They were in peer pairs. At the time of the current study, all animals were housed indoors in social pairs 24 hours per day, 7 days per week.

Behavioral Observations

Offspring participated in a series of behavioral and cognitive experiments from birth through four years of age, as described in our previous publications[35,36,38]. For correlations with metabolites we focus on stereotypic behaviors observed in captive macaques, including whole body motor stereotypies (i.e., circling, pacing, swaying, bouncing, flipping, and spinning) and self-injurious or self-directed behaviors (i.e., self-biting, self-hitting, self-clasping, and saluting). Stereotypic behaviors were quantified at three timepoints (i) Post-weaning (10 months of age), (ii) Juvenile (22 months of age) and (iii) Sub-adult (46 months of age). For behavioral observations each animal was placed individually in a large, unfamiliar cage and observed by trained observers who were blind to experimental conditions. Animals were observed for two 5-minute focal samples on 2 separate days. Due to the array of abnormal and repetitive behaviors observed in MIA animals at 10 and 22 months of age, we utilized a composite score of all repetitive behaviors[35]. More distinct behavioral categories emerged as animals aged, allowing for behaviors to be subcategorized at the 4-year time point as whole body versus self-directed.

Blood Collection and Peripheral Blood Mononuclear Cell (PBMC) stimulation

4 mL of peripheral blood was collected at sacrifice via an intravenous arm draw into acid-citrate-dextrose Vacutainers. To separate plasma from cellular components, blood was centrifuged at 2100 rpm for 10 mins. Plasma was aliquoted into 2 mL cryovials and stored in −80° C until cytokine and metabolome analysis was performed. Blood cells were layered on lymphocyte separation medium (Corning; Manassas, VA) and PBMCs were separated by gradient centrifugation. PBMC were washed twice with Hanks Balanced Salt Solution (Corning; Manassas, VA) and live cells were counted. PBMC concentrations were adjusted to a concentration of 1 x 10^6 cells/mL in complete media (RPMI 1640 (Invitrogen; Carlsbad, CA) with 10% Fetal Bovine Serum (Corning; Manassas, VA), 100 IU/ml penicillin (Invitrogen; Carlsbad, CA) and 100 IU/ml streptomycin (Invitrogen; Carlsbad, CA), 1% L-glutamine (Invitrogen; Carlsbad, CA)). Cells were cultured for 48 hours, after which supernatants were collected and stored at −80° C until analysis within a few months.

Tissue Collection and Cell Isolations

Animals were euthanized under the care of California National Primate Research Center veterinary staff at approximately four years of age. Out of consideration of the precious nature of NHPs, 3 (out of original 11) control animals were not euthanized, one of which had no metabolomics performed on plasma due to sample thawing. The brain was removed and one hemisphere from each animal was flash frozen in liquid nitrogen. Frozen hemispheres were stored at −80° C until they could be sectioned. Small tissue sections from the hippocampus, anterior cingulate, and prefrontal cortex were placed on a cold mortar with liquid nitrogen and compressed into a powder using a cold pestle. The powdered brain sections were transferred to a pre-weighed 15 mL conical tube, weighed and 10 volumes of cell lysis buffer was added. Samples were vortexed briefly and incubated on ice for 20 mins with intermittent agitation. After incubation samples were sonicated for 30 secs and centrifuged at 20,000g for 20 mins at 4° C. Supernatants were collected and stored at −80° C until cytokine analysis. 10-centimeter sections of the duodenum, jejunum, ileum, and colon were removed. 4-mL of intestinal contents were collected using sterile technique, placed into vials and flash frozen immediately. A mucosal scraping was collected from each section, an incision was made perpendicular to cut opened the intestinal section lengthwise, intestine was held with sterile forceps, while the lumen was scraped with a sterile slide. A sterile scoopula was used to place mucus into cryovials. Samples were flash frozen on dry ice and stored at −80° C until analysis. Intraepithelial lymphocytes and lamina propria lymphocytes were collected from intestinal tissue sections following standard digestion and isolation protocols. Intestinal sections were rinsed with 50 mL of cold PBS, excess connective tissue and fat were removed, and the 10 cm sections were cut into smaller pieces using 2 disposable scalpels. The tissue was then transferred to a 125 mL Erlenmeyer flask with 50 mL of IEL digestion media (Calcium and magnesium free Hanks Balanced Saline Solution (HBSS) with 1mM EDTA and 0.5 mM dithiothreitol, adjusted to pH 7.4) and incubated for 30 mins at 37° C. After 30 mins samples were strained through a size 40 steel mesh strainer to collect undigested pieces. The supernatant containing IELs from the first digestion was washed with 50 mL of PBS and centrifuged at 2000 RPM for 5 min. The undigested pieces were placed back into the Erlenmeyer flask with another 50 mL of IEL digestion media and the incubation and straining process was repeated a second time.

IELs were pooled from both digestions. The remaining tissue pieces were placed on a sterile petri dish and cut into 2-3 mm pieces. These pieces were placed in a 125 mL Erlenmeyer flask with 50 mL of prewarmed LPL media (RPMI with 3.85 wünsch units of Liberase TM). Samples were incubated for 30 mins at 37° C. After incubation a 10 mL pipet was used to break up tissue pieces by pipetting up and down. Samples were then poured over a 40 μm strainer into a 50 mL conical. Remaining tissue pieces were placed back into the Erlenmeyer flask with a fresh aliquot of LPL media for a second incubation. Cells collected from both the first and second LPL digestion were pooled together and washed twice with 50 mL of PBS. IEL and LPL cell suspensions were resuspended in 15 mL of complete RPMI, layered over a 35/60 percoll gradient, and centrifuged at 2500 RPM for 20 mins. Lymphocytes were collected at the 35/60 interface. Cells were washed with PBS and passed through 60 cc syringe barrels that were loosely packed with glass wool to remove excess mucus. The flow through was collected, cells pelleted by centrifuging at 2100 for 10 mins and resuspended in complete RPMI. 5 x 10^5 cells were plated per well of a 48 well plate and cultured in media for 24 hrs. Supernatants were collected and stored at −80 C until cytokine analysis.

Cytokine Analysis

Cytokine concentrations of the supernatants of stimulated cells, plasma, and brain regions (all prepared from fresh samples and stored at −80 C after processing) were determined by using a commercially available multiplexing bead immunoassays assay designed to analyze non-human primate cytokines (Millipore, Billerica, MA) (Supplementary Tables S17–S20). Cytokines analyzed included: Granulocyte Macrophage Colony Stimulating Factor (GM-CSF), Granulocyte Colony Stimulating Factor (G-CSF), IFNγ, Interleukin (IL)-1β, IL-2, IL-4, IL-5, IL-6, chemokine (C-X-C motif) ligand (CXCL)-8, IL-10, IL-12p40, IL-13, IL-17, chemokine (C-C motif) ligand (CCL)-2, CCL-3,CCL-4 and tumor necrosis factor (TNF)α. Samples were processed according to manufacturer's protocols and guidelines. Briefly, 25 μL of sample was incubated with antibody-immobilized beads. Following incubation, wells were washed and then samples were incubated with detection antibodies followed by the addition of streptavidin-phycoerythrin. After streptavidin-phycoerthrin incubation, wells were washed, and beads were resuspended with sheath fluid. Analysis of the bead sets was run on a Bio-Plex 200 system (Bio-Rad Laboratories, Inc.). Unknown sample cytokine concentrations were determined by Bio-Plex Manager software; calculations were based on a standard curve of known concentration provided in the kit by the manufacturer. Values of sample cytokines are expressed in pg/mL and have the following detection range: IL-4: (4.9 - 20,000 pg/mL); IL-10 (12.2 - 50,000 pg/mL); GM-CSF, G-CSF, IFNγ, IL-1β, IL-2, IL-5, IL-6, CXCL-8, IL-12p40, IL-13, IL-17, CCL-2, CCL-3, CCL-4, TNFα (2.4 - 10,000 pg/mL). Sample concentrations that were below the limit of detection were given a proxy value as half the limit of detection for statistical comparisons.

Ultrahigh Performance Liquid Chromatography-Tandem Mass Spectroscopy (UPLC-MS/MS):

Metabolomics was carried out (samples were stored without disruption for 4 years at −80C), by Metabolon, Inc. (Morrisville, NC) as follows: all methods utilized a Waters ACQUITY ultra-performance liquid chromatography (UPLC) and a Thermo Scientific Q-Exactive high resolution/accurate mass spectrometer interfaced with a heated electrospray

ionization (HESI-II) source and Orbitrap mass analyzer operated at 35,000 mass resolution. To precipitate proteins from solution, samples were shaken vigorously with methanol for two minutes (Glen Mills GenoGrinder 2000) followed by centrifugation. Extracts were partitioned into five aliquots and a TurboVap® (Zymark) was briefly used to remove the organic solvent. For each sample, four separate analyses were conducted using two reverse phase (RP)/UPLC-MS/MS methods with positive ion mode electrospray ionization (ESI), RP/UPLC-MS/MS with negative ion mode ESI, and HILIC/UPLC-MS/MS with negative ion mode ESI. The first aliquot was analyzed using acidic positive ion conditions, optimized for hydrophilic compounds. In this method, the extract was gradient eluted from a C18 column (Waters UPLC BEH C18-2.1x100 mm, 1.7 μm) using water and methanol, containing 0.05% perfluoropentanoic acid (PFPA) and 0.1% formic acid (FA). The second aliquot was also analyzed using acidic positive ion conditions but chromatographically optimized for hydrophobic compounds. In this method, the extract was gradient eluted from the same aforementioned C18 column using methanol, acetonitrile, water, 0.05% PFPA and 0.01% FA and was operated at an overall higher organic content. A third aliquot was analyzed using basic negative ion optimized conditions using a separate dedicated C18 column. The basic extracts were gradient eluted from the column using methanol and water, however with 6.5mM Ammonium Bicarbonate at pH 8. The fourth aliquot was analyzed via negative ionization following elution from a HILIC column (Waters UPLC BEH Amide 2.1x150 mm, 1.7 μm) using a gradient consisting of water and acetonitrile with 10mM Ammonium Formate, pH 10.8. The MS analysis alternated between MS and data-dependent MSn scans using dynamic exclusion. The scan range varied slightly between methods but covered 70-1000 m/z. Raw data was extracted, peak-identified and QC processed using Metabolon's hardware and software. Compounds were identified by comparison to library entries of purified standards or recurrent unknown entities. Peaks were quantified using area-under-the-curve. For studies spanning multiple days, a data normalization step was performed to correct variation resulting from instrument inter-day tuning differences. Each compound was corrected in run-day blocks by imputing values as needed, registering the medians to equal one (1.00), and log-normalizing each data point proportionately.

Statistical Analyses - Metabolomics

All poly ICLC offspring were grouped together for analysis as the MIA group. A two-way ANOVA was conducted for metabolites of each tissue for the treatment and sex variables followed by the Welch's two-sample post-hoc t-test and FDR correction of p-values for multiple comparisons. Visualization of metabolomic profiles in a low dimensional non-linear space was conducting via t-SNE (R package Rtsne[71]). Scaled and imputed values for all detected metabolites were used as input. Sparse partial least-squares discriminant analysis (sPLS-DA) was conducted using MetaboAnalystR (version 2.0)[72] to identify metabolites with the greatest potential for group discrimination.

Behavioral and Immune profile Correlations

Spearman's Rank correlation was calculated via cor.test (stats R package) for cytokine profiles and behavioral metrics of NHPs at four years of age. Values below the limit of detection (LOD) for bio-plex data are imputed as ½ the LOD. FDR correction of p-values

was then applied separately to all metabolite correlations to a specific cytokine or behavioral metric.

Pathway Enrichment Analysis

A hypergeometric *P*-value test (Eq. 1) was utilized for assessing sub-pathway overrepresentation of metabolites for statistical associations to group status and correlations to cytokine levels.

$$Score = -\log_{10}(1 - \sum_{i=0}^{k} \frac{\binom{m}{i}\binom{N-m}{n-i}}{\binom{N}{n}}) \quad (1)$$

where

- N is the number of total metabolites quantified
- n is the total number of significant metabolites
- m is the number of detected metabolites in the pathway
- k is the number of significant metabolites in the pathway.

An ANOVA contrast significance of ($p \leq 0.05$) was utilized for group status sub-pathway enrichment. For correlation enrichment scores, each unique cytokine and behavioral metric was analyzed for overrepresentation at the sub-pathway level, separately, utilizing ($q \leq 0.25$) to denote an association.

Fecal and Intestinal Microbiome Analysis

16S amplicon sequencing was conducted on stool and intestinal content from the jejunum and ileum. DNA was extracted using the DNeasy powersoil extraction kit (Qiagen), and the V4 rRNA gene was amplified via PCR using 515F 806R primers. Amplification was confirmed using electrophoresis and purified using the Quiaquick PCR kit (Qiagen). Samples were sequenced using a MiSeq v2 platform (Illumina) using 2 X 250 bp paired end reads. Demultiplexed reads were analyzed using QIIME2 (2021.8). Quality filtering, denoising, and merging of paired end reads was conducted using q2-dada2, trimming forward and reverse reads to 220 and 160 bp, respectively. Amplicon sequence variants (ASVs) were classified using QIIME classify-sklearn with a pretrained model on the 515F-806R regions of the Greengenes database (13_8 release) 99% OTUs. Statistical analysis and data visualization were generated in R (v4.1.0). For community composition analyses, read counts were rarified to 8,112, 12,607, and 34,869 for jejunum, ileum, and fecal samples, respectively, using the vegan R package[73]. Community diversity measures, including Observed ASVs, Shannon diversity, Gini dominance, Simpsons evenness, low-abundance rarity, Aitchison distance, and weighted and un-weighed UniFrac distance were determined using the microbiome, vegan[73] and phyloseq[74] R packages. Differential abundance was determined for ASVs, species, genera, and phyla using MaAsLin2[75]. Briefly, microbial features for each tissue were filtered for a prevalence of 10% followed by a trimmed mean of M-values normalization. Abundance profiles were then tested using

negative binomial regression using treatment status and sex as fixed effects. Correlations of ASV abundance to cytokine and metabolome profiles were conducted using Spearman's Rank-based correlation, described above.

Code availability

Scripts for data-visualization and statistical analysis of correlations, pathway enrichment, and microbiome analysis are available at: https://github.com/jboktor/NHP_MIA_Omics

RESULTS

MIA Offspring Display Differences in General Metabolic Pathways

Metabolomics were performed by Metabolon, Inc (Morrisville, NC) on the offspring of pregnant female rhesus macaques injected with the viral mimic polyinosinic:polycytidylic acid stabilized with poly-L-lysine (poly ICLC) to activate the maternal immune system during gestation (hereafter referred to as the MIA group), and were compared to control animals. Previously published data from the offspring in this study revealed immune, behavioral, and neuropathological features consistent with other preclinical MIA models and individuals with NDDs[31, 32, 34, 38]. At four years of age, samples were collected, including brain tissue, plasma, cerebrospinal fluid (CSF), feces, and scrapings from the intestinal mucosa along the jejunum, ileum, and colon, yielding group sizes of 8-10 control and 13 MIA offspring (see Methods for further description of groups). Tissues were analyzed via a global metabolite panel by UPLC-MS/MS, resulting in an extensive panel of identified metabolites with several metabolites measured at differential levels between NHP offspring groups (Fig. 1A). Due to the precious nature of the primate model and resulting limitations in power, few metabolites pass typical FDR thresholds. For exploratory purposes, we report metabolites deemed meaningful utilizing a p-value threshold of $p \leq 0.05$ for ANOVA contrasts, and FDR ≤ 0.2 for correlation associations. Samples clustered well according to tissue type, with surprising similarity between the small intestinal scraping, plasma, and CSF clusters as compared to the feces and colon scrapings (Fig. 1B).

To quantify alterations of broad metabolic processes we employed pathway enrichment analysis. Enrichment scores were summarized across all tissues and revealed emphasis on amino acid and lipid pathways (Fig. 1C), which were further examined at the tissue level and stratified by sex (Fig. 1D–1F and Supplementary Fig. S1A–S1H). Some metabolite levels were observed at differential levels in more than one tissue type, including pipecolate, creatine, cystine, hydantoin-5-propionic acid, N-acetylaspartylglutamate, and glucuronidated $C_{10}H_{18}O_2$ (Fig. 1G) and additional metabolites of interest across tissues in either males or females only (Supplementary Fig. S1I–S1J).

We also correlated all metabolites measured in this study with cytokine panels performed on plasma and PBMCs from blood, tissue from brain regions, and culture supernatant from isolated intestinal lymphocytes (Supplementary Tables S10–S12). We present an overview of the cytokine correlation as a summary enrichment score (Supplementary Fig. S2), with more specific data on correlations between metabolites and cytokines presented at the tissue level in the subsequent sections.

Metabolomic signatures could one day serve as biomarkers to aid in early and accurate diagnosis of NDDs. The characterization of metabolic perturbations could provide novel indications for the etiology of ASD, which remains largely enigmatic. To explore potential relationships between detected metabolites and the ASD-associated behavior phenotypes previously observed in these NHPs[31], we correlated whole body (pacing, bouncing, etc.), self-directed (self-biting or hitting, etc), the total of the two, or other stereotypic behaviors soon after weaning (6 mos.), during adolescence (2 years), and during adulthood (4 years) (Supplementary Table S9). We present these at the tissue level throughout the results section.

Plasma Levels of ASD-associated Metabolites

From a panel of 1429 identified metabolites, 25 metabolites were observed at differential levels in MIA plasma (Fig. 1A), with enrichments especially in carbohydrate and amino acid superpathways (Fig. 2A). Individual metabolites showing differences are displayed by volcano plot (Fig. 2B), such as the more than 2-fold higher level of retinal (or retinaldehyde), a vitamin A metabolite and precursor to retinoic acid.

To determine whether any structurally similar metabolites may be co-regulated, we performed correlations between all plasma metabolites (Supplementary Fig. S3A). In the top 25 correlations, many phenolic molecules, a structural class characteristically composed of microbially-modified dietary sources, are positively correlated with each other. Likewise, monohydroxy fatty acids and acyl-carnitines are positively correlated to each other but are negatively correlated with the phenolic metabolites.

The top ten metabolites that were the most distinguishing between MIA and control offspring samples were identified with sparse partial least squares discriminant analysis (sPLS-DA) (Fig. 2C, Supplementary Fig. S3B). Individual plots of relative values of four of the most discriminatory metabolites, allantoin, 3-hydroxyisobutyrate, guanidinoacetate, and azelate are provided (Fig. 2D) along with further select examples (Supplementary Fig. S3C).

Correlations between plasma metabolites and gut and brain cytokines reveal that IL-1β levels in plasma are associated with plasma metabolites in pentose, cofactors/vitamins, purine, and lipid pathways (Fig. 2E, Supplementary Fig. S4). Overall, the plasma results suggest that various metabolic changes could work in concert to impact the NHP MIA model.

CSF Levels of Mitochondrial Markers and Amino Acid Metabolites Differ

Cerebrospinal fluid (CSF) is a blood-brain filtrate produced in the brain's ventricles and contains ions, proteins, vitamins, and metabolites necessary for proper brain function[76]. CSF, at the interface between peripheral circulation and the central nervous system[77], is a more accurate representation of brain biochemistry and metabolism than the metabolome observed in systemic blood circulation[78, 79]. Pathway enrichment analysis of the analyzed CSF metabolome, which comprised 291 identified molecules, highlights metabolites associated with mitochondrial energy metabolism and several amino acid pathways (Fig. 3A). Of the 10 metabolites observed at differential levels in MIA vs control CSF, canonical intermediates and amino acid contributors to the TCA cycle (cysteine, serine, asparagine, proline), and metabolites peripherally related to mitochondrial metabolism through other

pathways (cysteine, asparagine), are decreased in MIA (Figure 3B–C). Indeed, in CSF we observed a higher level of asparagine and a lower level of cysteine (Fig 3C), metabolites crucial to urea and glutathione pathways[80] respectively (Fig 3A).

We also observed an increase in the sulfate-conjugated form of 3-methoxytyramine (3-MT), a neuroactive dopamine derivative, in the MIA group (Fig. 3B and 3C). The additional amino acids we measured at differential levels between groups in our dataset are also neuroactive (serine, cysteine, proline) or are precursors to neuroactive compounds (asparagine)[81]. We observed very limited correlations between CSF metabolites and cytokines and behavior scores (Supplementary Fig. S5, Supplementary Table S3). As a whole, these data indicate a possible consequence of altered brain amino acid and mitochondrial energy metabolism in response to MIA.

Fecal Levels of Metabolites in Lysine and Other Pathways Differ and Microbial Profiles Show Modest Shifts

Fecal metabolites can provide insight into host excretion and microbial metabolism. The complex, resident community of gut microbes, collectively termed the gut microbiota, interacts closely with dietary and host sources and exerts heavy influence on systemic metabolism[82]. Microbial manipulation has been used in preclinical studies to influence the abnormalities in MIA mice[10, 83] and may impact fecal metabolites; thus characterization of the metabolic makeup of fecal and intestinal samples along with samples more intuitively associated with neurological development, such as plasma and cerebrospinal fluid, was performed.

Out of the 637 identified fecal metabolites, we observed 12 differential levels that grouped mainly into lipid, energy, carbohydrate, nucleotide, and amino acid pathways (Fig. 4a and Supplementary Fig. S6a–c). Individual metabolites that stand out in the further downstream analyses include elevated levels of 3-carboxyadipate, beta-hydroxyisovalerate, and homocitrate, along with lower levels of ferulate (Fig. 4B–D).

To again examine potential co-regulation of metabolites, we performed correlations across all fecal metabolites between one another. In the top 25 correlations, many purine and pyrimidine nucleotide metabolites share a high positive correlation (Supplementary Fig. S6A). We observe negative correlations between two fecal acyl-carnitines and IL-10 levels in plasma (Fig. 4E, Supplementary Fig. S7). Two fecal metabolites, formiminoglutamate and homocitrulline, are positively correlated to more severe stereotypic behavior (Fig. 4F).

To explore the potential impact of treatment on NHP microbial communities, we performed 16S ribosomal RNA sequencing on fecal samples and ileum and jejunum scrapings, in addition to the metabolomics analysis. While we observe no significant differences in measure of diversity in stool (Fig S6D–E), numerous ASVs with significant associations with treatment status are detected (Fig. 4G). The most robust enrichments include *Prevotella, Oscillospira, Gemmiger formicilis*, *Roseburia faecis*, and *Ruminococcaceae*. Significant depletions include *Lactobacillus salivarus*, *Ruminococcus bromii, p-534-18B5, Dorea formicigenerans, Megasphaera, Eubacterium biforme, Treponema, and Blautia* (Fig. 4G). We performed correlations between stool sample 16S profiles with paired metabolome

data as well as cytokine abundance from cultured colonic lymphocytes and note multiple significant associations (Supplementary Fig. S7B). The *Dorea* genus, which has a poor capacity to degrade free amino acids and could thus influence the fecal metabolome, has shown either increased or decreased levels in human ASD microbiota sampling, depending on the cohort[84–88].

Metabolite Levels in Intestinal Scraping Samples Differ in Purine and Lipid Pathways

The gastrointestinal (GI) tract is a diverse interface between the host and environmental factors such as the microbiome and diet, which converge to influence intestinal as well as systemic metabolism, even in the brain[82, 89, 90]. Passing longitudinally down the gastrointestinal tract, host physiology and resident microbial populations vary greatly, so we collected three successive regions of scrapings, yielding 1062 identified metabolites, in order to capture a comprehensive metabolic snapshot along the intestine at the jejunum, ileum, and colon.

The small intestine is responsible for breakdown and absorption of simple nutrients[91], and in our jejunum and ileum samples, we see variation in 12 and 30 metabolites, respectively, that may reflect differences in these functions, including changes primarily to carbohydrate, lipid, and amino acid pathways (Fig. 5A–E, Supplementary Tables S7–S8). The purine metabolites, xanthine and its precursor, hypoxanthine, are both found at over a 10 and 6-fold increase, respectively, in MIA ileal samples, consistent with aberrant purine metabolism within these animals (Fig. 5B–C).

The changes in pathways of colon scrapings are dominated by lipids, many of which are directly produced or influenced by microbes, such as secondary bile acids. However, of the 14 differentially abundant metabolites, the most striking difference between MIA and control colon scrapings is gentisate, which is over 16-fold lower in MIA samples (Fig. S9A–S9C).

Levels of the cytokine IL5 in the hippocampus and plasma correlate with metabolites in these scrapings, primarily lipids (Fig. S8A,C, S9D, S10, Supplementary Tables S7–S8). Lipid metabolites measured in the jejunum, including stearoyl sphingomyelin and stearoyl-linoleoyl-glycerol positively correlate with stereotypic severity (Supplementary Fig. S8D). 1-methyl-4-imidazoleacetate, carboxyethyl-GABA, N-acetylglutamine, and isoleucine levels in the colon negatively correlate with stereotypic severity (Supplementary Fig. S9E).

Microbial community profiling of ileum and jejunum samples revealed trending depletion of observed taxa and Shannon diversity in MIA samples in the ileum but not the jejunum (Fig. S8E–H). Differential abundance testing of ASVs showed a phylogenetically diverse array of microbes to be enriched in MIA ileum and jejunum samples (Fig. 5G–H, Supplementary Table S14). Correlations between intestinal microbial profiles and paired sample metabolomes highlight several associations between metabolites of known microbial origin and microbial abundance including indoles, phenols, and sulfated steroid compounds (Fig. S11, Supplementary Table S15). Cytokine profile correlations with microbial abundance indicate a subset of ASVs with strong associations across the panel of detected proteins (Fig. S11, Supplementary Table S16). Intestinal scrapings are difficult

to obtain in ASD individuals, making this NHP sample set invaluable as a proxy to identify potential mechanisms of MIA for further study.

DISCUSSION

In this study, samples spanning multiple locations in a NHP MIA model, including plasma, CSF, feces, and intestinal scrapings, were analyzed by an extensive metabolomics panel. The resulting metabolic profiles showed the highest number of differentially abundant metabolites between MIA and control offspring in plasma. Globally, a common thread of altered nucleotide metabolism was observed in multiple tissues, most predominantly in the 10- and 6-fold elevation of xanthine and hypoxanthine in MIA ileal samples. This is consistent with hypotheses that aberrant purine metabolism plays a role in NDDs[92–94].

Several metabolites appear to be particularly key in this model and have association with ASD in preclinical and clinical contexts (Table 1). Retinal levels were over 2-fold elevated in MIA plasma. Retinal signaling and development is affected in more than one ASD mouse model as well as in some ASD individuals, with associations to hypersensitivity to sensory stimuli [95–97]. In fact, murine MIA dysregulates genes in the fetal brain that are important for eye retina development, are associated with the metabolite retinal, and regulate aspects of axonal neurite outgrowth during development [39, 98].

In the CSF, altered levels of multiple amino acids, including serine, cysteine, proline and asparagine, could indicate dysregulated neurotransmitter levels. Due to its reflection of metabolite production in the brain[99], analysis of the CSF metabolome provides information on the biochemical environment within the central nervous system, specifically in the context of diseases affecting the brain, so these modest differences may be meaningful[100–103].

Gastrointestinal samples analyzed herein mainly demonstrated differential levels of amino acid, purine, and lipid pathway metabolites, and highlight the need to compare samples from equivalent intestinal regions to draw conclusions across studies, as the various sites differed from each other. 3-carboxyadipate, which is increased in MIA feces, is a lysine metabolite. Along with other differences in lysine pathway metabolites, such as increased levels of homocitrate and lower levels of pipecolate and 2-hydroxyglutarate, this implicates broad alterations to lysine metabolism in MIA samples (Fig. 4B, D and Supplementary Table S5). In fact, 2-hydroxyglutarate is also decreased in female ileum scrapings (Supplementary Table S5), and other lysine metabolites also display differential levels in comparisons within plasma, CSF, and jejunum, ileum and colon scrapings (Supplementary Tables S1–S8).

In humans, ASD diagnosis ratios heavily favor males[104]. Interestingly, sex differences were observed in our study, with differences in MIA metabolic profiles between our male and female dataset. However, the number of differential metabolites in MIA males and females were mostly similar (Fig. 1A). These differences will require further study with additional, potentially larger cohorts to validate the contribution of these metabolites to the model. In fact, sample size is a limitation across this study, and to all NHP studies, due to their precious nature.

Other limitations of this study include the possibility of false significance assigned to some metabolites due to the large number of identified molecules and relatively small sample size, requiring the need for reproduction of these results in additional cohorts of animals. Furthermore, it is impossible to conclude from this study whether any of these metabolites play a causal role in MIA phenotypes in NHPs, may serve as biomarkers, or may be purely associated with the model. Future studies assessing causality in preclinical and clinical contexts are warranted.

There are many indications that metabolic therapies improve symptoms of ASD in humans and animal models[105–108]. For instance, implementation of a ketogenic diet has been associated with increased levels of 3-hydroxybutyrate and improved behavior[107]. Here, we observe lower levels of 3-hydroxyisobutyrate in MIA samples, which is an isomer of 3-hydroxybutyrate, a ketone body that is also lower in samples from ASD children.

The potential alterations observed in clinical ASD samples due to genetics, common GI symptoms, general dietary preferences of ASD children, and the complicating factors of medication and supplements could artificially drive some metabolite changes observed in human studies[109]. As a result, the MIA model has emerged as a translational tool that allows examination into the interaction between immune and environmental contributing factors, including microbial metabolic activity. Furthermore, NHPs mimic the human condition more closely than rodents, but metabolic changes in the NHP MIA model have not been previously studied. Utilizing a human-like, yet easily monitored model removes the innate variability of human metabolomics studies and provides a unique opportunity to study metabolic and microbial alterations relevant to neurodevelopment. Systemic host metabolism is greatly molded by dietary and microbial metabolites disseminating from the intestine, and gut physiology, function, and metabolism is reciprocally affected by the nervous system. This is exerted through bidirectional signaling through circulatory, gut, immune, and nervous system pathways, ultimately dictating changes in the brain and behavioral outputs[110–113]. However, causative relationships between global host metabolite levels and ASD symptoms have been difficult to define without a more complete host metabolome in translational models. This study supports the further investigation of metabolites as biomarkers and/or bioactive factors in ASD for improved diagnosis or therapeutic potential.

Supplementary Material

Refer to Web version on PubMed Central for supplementary material.

ACKNOWLEDGMENTS

This work was supported by grants from Autism Speaks (Grant #7567 to P.A., and S.K.M.); the Johnson Foundation (to P.A.); the Brain Foundation (to P.A. and to S.K.M.); NARSAD Foundation (to P.A.); Axial Biotherapeutics (to S.K.M.); and the National Institutes of Health (HD090214 to P.A.) and (MH100556 to S.K.M.). Development of the animal model was supported by a grant from the Simons Foundation to the late Dr. Paul Patterson (SFARI 9900060), with additional support provided by the base grant (RR00169) of the California National Primate Research Center (CNPRC), a gift from Ted and Ginger Jenkins and a UC Davis RISE Award (to P.A. and M.B.). We thank the veterinary and animal services staff of the CNPRC for care of the animals. Poly ICLC was kindly provided by Dr. Andres Salazar, MD, Oncovir, Washington D.C.

REFERENCES

1. Doernberg E, Hollander E. Neurodevelopmental Disorders (ASD and ADHD): DSM-5, ICD-10, and ICD-11. CNS Spectr. 2016;21:295–299. [PubMed: 27364515]
2. Baio J, Wiggins L, Christensen DL, Maenner MJ, Daniels J, Warren Z, et al. Prevalence of Autism Spectrum Disorder Among Children Aged 8 Years — Autism and Developmental Disabilities Monitoring Network, 11 Sites, United States, 2014. MMWR Surveill Summ. 2018;67:1–23.
3. Gaugler T, Klei L, Sanders SJ, Bodea CA, Goldberg AP, Lee AB, et al. Most genetic risk for autism resides with common variation. Nat Genet. 2014;46:881–885. [PubMed: 25038753]
4. Sandin S, Lichtenstein P, Kuja-Halkola R, Larsson H, Hultman CM, Reichenberg A. The Familial Risk Of Autism. JAMA. 2014;311:1770–1777. [PubMed: 24794370]
5. Gardener H, Spiegelman D, Buka SL. Prenatal Risk Factors for Autism: A Comprehensive Meta-analysis. Br J Psychiatry J Ment Sci. 2009;195:7–14.
6. Bilbo SD, Block CL, Bolton JL, Hanamsagar R, Tran PK. Beyond infection - Maternal immune activation by environmental factors, microglial development, and relevance for autism spectrum disorders. Exp Neurol. 2018;299:241–251. [PubMed: 28698032]
7. Bromley RL, Mawer GE, Briggs M, Cheyne C, Clayton-Smith J, García-Fiñana M, et al. The prevalence of neurodevelopmental disorders in children prenatally exposed to antiepileptic drugs. J Neurol Neurosurg Psychiatry. 2013;84:637–643. [PubMed: 23370617]
8. Roullet FI, Wollaston L, Decatanzaro D, Foster JA. Behavioral and molecular changes in the mouse in response to prenatal exposure to the anti-epileptic drug valproic acid. Neuroscience. 2010;170:514–522. [PubMed: 20603192]
9. Coretti L, Cristiano C, Florio E, Scala G, Lama A, Keller S, et al. Sex-related alterations of gut microbiota composition in the BTBR mouse model of autism spectrum disorder. Sci Rep. 2017;7:srep45356.
10. Hsiao EY, McBride SW, Hsien S, Sharon G, Hyde ER, McCue T, et al. Microbiota Modulate Behavioral and Physiological Abnormalities Associated with Neurodevelopmental Disorders. Cell. 2013;155:1451–1463. [PubMed: 24315484]
11. Lim JS, Lim MY, Choi Y, Ko G. Modeling environmental risk factors of autism in mice induces IBD-related gut microbial dysbiosis and hyperserotonemia. Mol Brain. 2017;10. [PubMed: 28385162]
12. Liu F, Horton-Sparks K, Hull V, Li RW, Martínez-Cerdeño V. The valproic acid rat model of autism presents with gut bacterial dysbiosis similar to that in human autism. Mol Autism. 2018;9:61. [PubMed: 30555669]
13. Tabouy L, Getselter D, Ziv O, Karpuj M, Tabouy T, Lukic I, et al. Dysbiosis of microbiome and probiotic treatment in a genetic model of autism spectrum disorders. Brain Behav Immun. 2018;73:310–319. [PubMed: 29787855]
14. Pulikkan J, Mazumder A, Grace T. Role of the Gut Microbiome in Autism Spectrum Disorders. Adv Exp Med Biol. 2019;1118:253–269. [PubMed: 30747427]
15. Sharon G, Cruz NJ, Kang D-W, Gandal MJ, Wang B, Kim Y-M, et al. Human Gut Microbiota from Autism Spectrum Disorder Promote Behavioral Symptoms in Mice. Cell. 2019;177:1600–1618.e17. [PubMed: 31150625]
16. Malkova NV, Yu CZ, Hsiao EY, Moore MJ, Patterson PH. Maternal immune activation yields offspring displaying mouse versions of the three core symptoms of autism. Brain Behav Immun. 2012;26:607–616. [PubMed: 22310922]
17. Haida O, Al Sagheer T, Balbous A, Francheteau M, Matas E, Soria F, et al. Sex-dependent behavioral deficits and neuropathology in a maternal immune activation model of autism. Transl Psychiatry. 2019;9:1–12. [PubMed: 30664621]
18. Amodeo DA, Lai C-Y, Hassan O, Mukamel EA, Behrens MM, Powell SB. Maternal immune activation impairs cognitive flexibility and alters transcription in frontal cortex. Neurobiol Dis. 2019;125:211–218. [PubMed: 30716470]
19. Schwartzer JJ, Careaga M, Onore CE, Rushakoff JA, Berman RF, Ashwood P. Maternal immune activation and strain specific interactions in the development of autism-like behaviors in mice. Transl Psychiatry. 2013;3:e240. [PubMed: 23481627]

20. Smith SEP, Li J, Garbett K, Mirnics K, Patterson PH. Maternal Immune Activation Alters Fetal Brain Development through Interleukin-6. J Neurosci. 2007;27:10695–10702. [PubMed: 17913903]
21. Choi GB, Yim YS, Wong H, Kim S, Kim H, Kim SV, et al. The maternal interleukin-17a pathway in mice promotes autism-like phenotypes in offspring. Science. 2016;351:933–939. [PubMed: 26822608]
22. Hsiao EY, McBride SW, Chow J, Mazmanian SK, Patterson PH. Modeling an autism risk factor in mice leads to permanent immune dysregulation. Proc Natl Acad Sci. 2012;109:12776–12781. [PubMed: 22802640]
23. Lammert CR, Frost EL, Bolte AC, Paysour MJ, Shaw ME, Bellinger CE, et al. Cutting Edge: Critical Roles for Microbiota-Mediated Regulation of the Immune System in a Prenatal Immune Activation Model of Autism. J Immunol. 2018;201:845–850. [PubMed: 29967099]
24. A Hypothesis-Based Approach: The Use of Animals in Mental Health Research. Natl Inst Ment Health NIMH. https://www.nimh.nih.gov/about/director/messages/2019/a-hypothesis-based-approach-the-use-of-animals-in-mental-health-research. Accessed 23 June 2022.
25. Lombardo MV, Moon HM, Su J, Palmer TD, Courchesne E, Pramparo T. Maternal immune activation dysregulation of the fetal brain transcriptome and relevance to the pathophysiology of autism spectrum disorder. Mol Psychiatry. 2018;23:1001–1013. [PubMed: 28322282]
26. Shi L, Smith SEP, Malkova N, Tse D, Su Y, Patterson PH. Activation of the maternal immune system alters cerebellar development in the offspring. Brain Behav Immun. 2009;23:116–123. [PubMed: 18755264]
27. Corradini I, Focchi E, Rasile M, Morini R, Desiato G, Tomasoni R, et al. Maternal Immune Activation Delays Excitatory-to-Inhibitory Gamma-Aminobutyric Acid Switch in Offspring. Biol Psychiatry. 2018;83:680–691. [PubMed: 29146047]
28. Li Y, Missig G, Finger BC, Landino SM, Alexander AJ, Mokler EL, et al. Maternal and Early Postnatal Immune Activation Produce Dissociable Effects on Neurotransmission in mPFC–Amygdala Circuits. J Neurosci. 2018;38:3358–3372. [PubMed: 29491010]
29. Bergdolt L, Dunaevsky A. Brain changes in a maternal immune activation model of neurodevelopmental brain disorders. Prog Neurobiol. 2019;175:1–19. [PubMed: 30590095]
30. Careaga M, Murai T, Bauman MD. Maternal immune activation and autism spectrum disorder: From rodents to nonhuman and human primates. Biol Psychiatry. 2017;81:391–401. [PubMed: 28137374]
31. Bauman MD, Iosif A-M, Smith SEP, Bregere C, Amaral DG, Patterson PH. Activation of the Maternal Immune System During Pregnancy Alters Behavioral Development of Rhesus Monkey Offspring. Biol Psychiatry. 2014;75:332–341. [PubMed: 24011823]
32. Machado CJ, Whitaker AM, Smith SEP, Patterson PH, Bauman MD. Maternal Immune Activation in Nonhuman Primates Alters Social Attention in Juvenile Offspring. Biol Psychiatry. 2015;77:823–832. [PubMed: 25442006]
33. Willette AA, Lubach GR, Knickmeyer RC, Short SJ, Styner M, Gilmore JH, et al. Brain enlargement and increased behavioral and cytokine reactivity in infant monkeys following acute prenatal endotoxemia. Behav Brain Res. 2011;219:108–115. [PubMed: 21192986]
34. Rose DR, Careaga M, Van de Water J, McAllister K, Bauman MD, Ashwood P. Long-term altered immune responses following fetal priming in a non-human primate model of maternal immune activation. Brain Behav Immun. 2017;63:60–70. [PubMed: 27876552]
35. Short SJ, Lubach GR, Karasin AI, Olsen CW, Styner M, Knickmeyer RC, et al. Maternal Influenza Infection During Pregnancy Impacts Postnatal Brain Development in the Rhesus Monkey. Biol Psychiatry. 2010;67:965–973. [PubMed: 20079486]
36. Vlasova RM, Iosif A-M, Ryan AM, Funk LH, Murai T, Chen S, et al. Maternal Immune Activation during Pregnancy Alters Postnatal Brain Growth and Cognitive Development in Nonhuman Primate Offspring. J Neurosci. 2021;41:9971–9987. [PubMed: 34607967]
37. Bauman MD, Lesh TA, Rowland DJ, Schumann CM, Smucny J, Kukis DL, et al. Preliminary evidence of increased striatal dopamine in a nonhuman primate model of maternal immune activation. Transl Psychiatry. 2019;9:1–8. [PubMed: 30664621]

38. Weir RK, Forghany R, Smith SEP, Patterson PH, McAllister AK, Schumann CM, et al. Preliminary evidence of neuropathology in nonhuman primates prenatally exposed to maternal immune activation. Brain Behav Immun. 2015;48:139–146. [PubMed: 25816799]
39. Garbett KA, Hsiao EY, Kálmán S, Patterson PH, Mirnics K. Effects of maternal immune activation on gene expression patterns in the fetal brain. Transl Psychiatry. 2012;2:e98. [PubMed: 22832908]
40. Oskvig DB, Elkahloun AG, Johnson KR, Phillips TM, Herkenham M. Maternal immune activation by LPS selectively alters specific gene expression profiles of interneuron migration and oxidative stress in the fetus without triggering a fetal immune response. Brain Behav Immun. 2012;26:623–634. [PubMed: 22310921]
41. Adams JB, Vargason T, Kang D-W, Krajmalnik-Brown R, Hahn J. Multivariate Analysis of Plasma Metabolites in Children with Autism Spectrum Disorder and Gastrointestinal Symptoms Before and After Microbiota Transfer Therapy. Processes. 2019;7:806.
42. Bitar T, Mavel S, Emond P, Nadal-Desbarats L, Lefèvre A, Mattar H, et al. Identification of metabolic pathway disturbances using multimodal metabolomics in autistic disorders in a Middle Eastern population. J Pharm Biomed Anal. 2018;152:57–65. [PubMed: 29414019]
43. Gevi F, Zolla L, Gabriele S, Persico AM. Urinary metabolomics of young Italian autistic children supports abnormal tryptophan and purine metabolism. Mol Autism. 2016;7. [PubMed: 26788284]
44. Kang D-W, Ilhan ZE, Isern NG, Hoyt DW, Howsmon DP, Shaffer M, et al. Differences in fecal microbial metabolites and microbiota of children with autism spectrum disorders. Anaerobe. 2018;49:121–131. [PubMed: 29274915]
45. Kuwabara H, Yamasue H, Koike S, Inoue H, Kawakubo Y, Kuroda M, et al. Altered metabolites in the plasma of autism spectrum disorder: a capillary electrophoresis time-of-flight mass spectroscopy study. PloS One. 2013;8:e73814. [PubMed: 24058493]
46. Lussu M, Noto A, Masili A, Rinaldi AC, Dessì A, Angelis MD, et al. The urinary 1H-NMR metabolomics profile of an italian autistic children population and their unaffected siblings. Autism Res. 2017;10:1058–1066. [PubMed: 28296209]
47. Orozco JS, Hertz-Picciotto I, Abbeduto L, Slupsky CM. Metabolomics analysis of children with autism, idiopathic-developmental delays, and Down syndrome. Transl Psychiatry. 2019;9:243. [PubMed: 31582732]
48. West PR, Amaral DG, Bais P, Smith AM, Egnash LA, Ross ME, et al. Metabolomics as a Tool for Discovery of Biomarkers of Autism Spectrum Disorder in the Blood Plasma of Children. PLoS ONE. 2014;9:e112445. [PubMed: 25380056]
49. Yap IKS, Angley M, Veselkov KA, Holmes E, Lindon JC, Nicholson JK. Urinary metabolic phenotyping differentiates children with autism from their unaffected siblings and age-matched controls. J Proteome Res. 2010;9:2996–3004. [PubMed: 20337404]
50. Smith AM, King JJ, West PR, Ludwig MA, Donley ELR, Burrier RE, et al. Amino Acid Dysregulation Metabotypes: Potential Biomarkers for Diagnosis and Individualized Treatment for Subtypes of Autism Spectrum Disorder. Biol Psychiatry. 2019;85:345–354. [PubMed: 30446206]
51. Altieri L, Neri C, Sacco R, Curatolo P, Benvenuto A, Muratori F, et al. Urinary p-cresol is elevated in small children with severe autism spectrum disorder. Biomark Biochem Indic Expo Response Susceptibility Chem. 2011;16:252–260.
52. Emond P, Mavel S, Aïdoud N, Nadal-Desbarats L, Montigny F, Bonnet-Brilhault F, et al. GC-MS-based urine metabolic profiling of autism spectrum disorders. Anal Bioanal Chem. 2013;405:5291–5300. [PubMed: 23571465]
53. Gabriele S, Sacco R, Cerullo S, Neri C, Urbani A, Tripi G, et al. Urinary p-cresol is elevated in young French children with autism spectrum disorder: a replication study. Biomark Biochem Indic Expo Response Susceptibility Chem. 2014;19:463–470.
54. Lis AW, Mclaughlin I, Mpclaughlin RK, Lis EW, Stubbs EG. Profiles of ultraviolet-absorbing components of urine from autistic children, as obtained by high-resolution ion-exchange chromatography. Clin Chem. 1976;22:1528–1532. [PubMed: 954199]
55. Nadal-Desbarats L, Aïdoud N, Emond P, Blasco H, Filipiak I, Sarda P, et al. Combined ^{1}H-NMR and ^{1}H–^{13}C HSQC-NMR to improve urinary screening in autism spectrum disorders. The Analyst. 2014;139:3460–3468. [PubMed: 24841505]

56. El-Ansary A, Al-Ayadhi L. Lipid mediators in plasma of autism spectrum disorders. Lipids Health Dis. 2012;11:160. [PubMed: 23170784]
57. El-Ansary AK, Bacha AGB, Al-Ayahdi LY. Impaired plasma phospholipids and relative amounts of essential polyunsaturated fatty acids in autistic patients from Saudi Arabia. Lipids Health Dis. 2011;10:63. [PubMed: 21513514]
58. James SJ, Cutler P, Melnyk S, Jernigan S, Janak L, Gaylor DW, et al. Metabolic biomarkers of increased oxidative stress and impaired methylation capacity in children with autism. Am J Clin Nutr. 2004;80:1611–1617. [PubMed: 15585776]
59. Lv Q-Q, You C, Zou X-B, Deng H-Z. Acyl-carnitine, C5DC, and C26 as potential biomarkers for diagnosis of autism spectrum disorder in children. Psychiatry Res. 2018;267:277–280. [PubMed: 29945069]
60. Mostafa GA, AL-Ayadhi LY. Reduced levels of plasma polyunsaturated fatty acids and serum carnitine in autistic children: relation to gastrointestinal manifestations. Behav Brain Funct BBF. 2015;11. [PubMed: 25871636]
61. Pastural E, Ritchie S, Lu Y, Jin W, Kavianpour A, Khine Su-Myat K, et al. Novel plasma phospholipid biomarkers of autism: mitochondrial dysfunction as a putative causative mechanism. Prostaglandins Leukot Essent Fatty Acids. 2009;81:253–264. [PubMed: 19608392]
62. Wang H, Liang S, Wang M, Gao J, Sun C, Wang J, et al. Potential serum biomarkers from a metabolomics study of autism. J Psychiatry Neurosci. 2016;41:27–37. [PubMed: 26395811]
63. Wang L, Christophersen CT, Sorich MJ, Gerber JP, Angley MT, Conlon MA. Elevated Fecal Short Chain Fatty Acid and Ammonia Concentrations in Children with Autism Spectrum Disorder. Dig Dis Sci. 2012;57:2096–2102. [PubMed: 22535281]
64. Cheng N, Rho JM, Masino SA. Metabolic Dysfunction Underlying Autism Spectrum Disorder and Potential Treatment Approaches. Front Mol Neurosci. 2017;10. [PubMed: 28197071]
65. Azhari A, Azizan F, Esposito G. A systematic review of gut-immune-brain mechanisms in Autism Spectrum Disorder. Dev Psychobiol. 2018. 6 December 2018. 10.1002/dev.21803.
66. Cozzolino R, De Magistris L, Saggese P, Stocchero M, Martignetti A, Di Stasio M, et al. Use of solid-phase microextraction coupled to gas chromatography–mass spectrometry for determination of urinary volatile organic compounds in autistic children compared with healthy controls. Anal Bioanal Chem. 2014;406:4649–4662. [PubMed: 24828982]
67. Ming X, Stein TP, Barnes V, Rhodes N, Guo L. Metabolic Perturbance in Autism Spectrum Disorders: A Metabolomics Study. J Proteome Res. 2012;11:5856–5862. [PubMed: 23106572]
68. Noto A, Fanos V, Barberini L, Grapov D, Fattuoni C, Zaffanello M, et al. The urinary metabolomics profile of an Italian autistic children population and their unaffected siblings. J Matern-Fetal Neonatal Med Off J Eur Assoc Perinat Med Fed Asia Ocean Perinat Soc Int Soc Perinat Obstet. 2014;27 Suppl 2:46–52.
69. Shaw W, Kassen E, Chaves E. Increased urinary excretion of analogs of Krebs cycle metabolites and arabinose in two brothers with autistic features. Clin Chem. 1995;41:1094–1104. [PubMed: 7628083]
70. Naviaux JC, Schuchbauer MA, Li K, Wang L, Risbrough VB, Powell SB, et al. Reversal of autism-like behaviors and metabolism in adult mice with single-dose antipurinergic therapy. Transl Psychiatry. 2014;4:e400–e400. [PubMed: 24937094]
71. Krijthe J, van der Maaten L, Krijthe MJ. Package 'Rtsne'. GitHub; 2018.
72. Xia J, Mandal R, Sinelnikov IV, Broadhurst D, Wishart DS. MetaboAnalyst 2.0—a comprehensive server for metabolomic data analysis. Nucleic Acids Res. 2012;40:W127–W133. [PubMed: 22553367]
73. Dixon P VEGAN, a package of R functions for community ecology. J Veg Sci. 2003;14:927–930.
74. McMurdie PJ, Holmes S. phyloseq: An R Package for Reproducible Interactive Analysis and Graphics of Microbiome Census Data. PLOS ONE. 2013;8:e61217. [PubMed: 23630581]
75. Mallick H, Rahnavard A, McIver LJ, Ma S, Zhang Y, Nguyen LH, et al. Multivariable Association Discovery in Population-scale Meta-omics Studies. 2021.
76. Spector R, Robert Snodgrass S, Johanson CE. A balanced view of the cerebrospinal fluid composition and functions: Focus on adult humans. Exp Neurol. 2015;273:57–68. [PubMed: 26247808]

77. Lun MP, Monuki ES, Lehtinen MK. Development and functions of the choroid plexus-cerebrospinal fluid system. Nat Rev Neurosci. 2015;16:445–457. [PubMed: 26174708]

78. Wishart DS, Lewis MJ, Morrissey JA, Flegel MD, Jeroncic K, Xiong Y, et al. The human cerebrospinal fluid metabolome. J Chromatogr B Analyt Technol Biomed Life Sci. 2008;871:164–173.

79. Perry TL, Jones RT. The amino acid content of human cerebrospinal fluid in normal individuals and in mental defectives. J Clin Invest. 1961;40:1363–1372. [PubMed: 13734593]

80. Mason S, Reinecke CJ, Solomons R. Cerebrospinal Fluid Amino Acid Profiling of Pediatric Cases with Tuberculous Meningitis. Front Neurosci. 2017;11:534. [PubMed: 29018323]

81. Billard J-M. D-Amino acids in brain neurotransmission and synaptic plasticity. Amino Acids. 2012;43:1851–1860. [PubMed: 22886346]

82. Sonnenburg JL, Bäckhed F. Diet–microbiota interactions as moderators of human metabolism. Nature. 2016;535:56–64. [PubMed: 27383980]

83. Kim S, Kim H, Yim YS, Ha S, Atarashi K, Tan TG, et al. Maternal gut bacteria promote neurodevelopmental abnormalities in mouse offspring. Nature. 2017;549:528–532. [PubMed: 28902840]

84. Strati F, Cavalieri D, Albanese D, De Felice C, Donati C, Hayek J, et al. New evidences on the altered gut microbiota in autism spectrum disorders. Microbiome. 2017;5:24. [PubMed: 28222761]

85. De Angelis M, Piccolo M, Vannini L, Siragusa S, De Giacomo A, Serrazzanetti DI, et al. Fecal microbiota and metabolome of children with autism and pervasive developmental disorder not otherwise specified. PloS One. 2013;8:e76993. [PubMed: 24130822]

86. Luna RA, Oezguen N, Balderas M, Venkatachalam A, Runge JK, Versalovic J, et al. Distinct Microbiome-Neuroimmune Signatures Correlate With Functional Abdominal Pain in Children With Autism Spectrum Disorder. Cell Mol Gastroenterol Hepatol. 2017;3:218–230. [PubMed: 28275689]

87. Iglesias-Vázquez L, Van Ginkel Riba G, Arija V, Canals J. Composition of Gut Microbiota in Children with Autism Spectrum Disorder: A Systematic Review and Meta-Analysis. Nutrients. 2020;12:792. [PubMed: 32192218]

88. Russell WR, Duncan SH, Scobbie L, Duncan G, Cantlay L, Calder AG, et al. Major phenylpropanoid-derived metabolites in the human gut can arise from microbial fermentation of protein. Mol Nutr Food Res. 2013;57:523–535. [PubMed: 23349065]

89. Koppel N, Rekdal VM, Balskus EP. Chemical transformation of xenobiotics by the human gut microbiota. Science. 2017;356:eaag2770. [PubMed: 28642381]

90. Obrenovich M, Flückiger R, Sykes L, Donskey C. The Co-Metabolism within the Gut-Brain Metabolic Interaction: Potential Targets for Drug Treatment and Design. CNS Neurol Disord Drug Targets. 2016;15:127–134. [PubMed: 26831263]

91. Karasov WH. Integrative physiology of transcellular and paracellular intestinal absorption. J Exp Biol. 2017;220:2495–2501. [PubMed: 28724701]

92. Naviaux RK, Zolkipli Z, Wang L, Nakayama T, Naviaux JC, Le TP, et al. Antipurinergic therapy corrects the autism-like features in the poly(IC) mouse model. PloS One. 2013;8:e57380. [PubMed: 23516405]

93. Fumagalli M, Lecca D, Abbracchio MP, Ceruti S. Pathophysiological Role of Purines and Pyrimidines in Neurodevelopment: Unveiling New Pharmacological Approaches to Congenital Brain Diseases. Front Pharmacol. 2017;8. [PubMed: 28154535]

94. Page T, Coleman M. Purine metabolism abnormalities in a hyperuricosuric subclass of autism. Biochim Biophys Acta. 2000;1500:291–296. [PubMed: 10699370]

95. Guimarães-Souza EM, Joselevitch C, Britto LRG, Chiavegatto S. Retinal alterations in a preclinical model of an autism spectrum disorder. Mol Autism. 2019;10:19. [PubMed: 31011411]

96. Pavăl D, Rad F, Rusu R, Niculae A-Ş, Colosi HA, Dobrescu I, et al. Low Retinal Dehydrogenase 1 (RALDH1) Level in Prepubertal Boys with Autism Spectrum Disorder: A Possible Link to Dopamine Dysfunction? Clin Psychopharmacol Neurosci. 2017;15:229–236. [PubMed: 28783931]

97. Zhang X, Piano I, Messina A, D'Antongiovanni V, Crò F, Provenzano G, et al. Retinal defects in mice lacking the autism-associated gene Engrailed-2. Neuroscience. 2019;408:177–190. [PubMed: 30980901]

98. Wang YH, Wang DW, Wu N, Wang Y, Yin ZQ. Alpha-crystallin promotes rat retinal neurite growth on myelin substrates in vitro. Ophthalmic Res. 2011;45:164–168. [PubMed: 20881446]

99. Hoffmann GF, Meier-Augenstein W, Stöckler S, Surtees R, Rating D, Nyhan WL. Physiology and pathophysiology of organic acids in cerebrospinal fluid. J Inherit Metab Dis. 1993;16:648–669. [PubMed: 8412012]

100. Oztan O, Garner JP, Constantino JN, Parker KJ. Neonatal CSF vasopressin concentration predicts later medical record diagnoses of autism spectrum disorder. Proc Natl Acad Sci. 2020;117:10609–10613. [PubMed: 32341146]

101. Stoessel D, Schulte C, Teixeira dos Santos MC, Scheller D, Rebollo-Mesa I, Deuschle C, et al. Promising Metabolite Profiles in the Plasma and CSF of Early Clinical Parkinson's Disease. Front Aging Neurosci. 2018;10:51. [PubMed: 29556190]

102. Jiménez-Jiménez FJ, Alonso-Navarro H, García-Martín E, Agúndez JAG. Cerebrospinal fluid biochemical studies in patients with Parkinson's disease: toward a potential search for biomarkers for this disease. Front Cell Neurosci. 2014;8:369. [PubMed: 25426023]

103. Czech C, Berndt P, Busch K, Schmitz O, Wiemer J, Most V, et al. Metabolite Profiling of Alzheimer's Disease Cerebrospinal Fluid. PLOS ONE. 2012;7:e31501. [PubMed: 22359596]

104. Loomes R, Hull L, Mandy WPL. What Is the Male-to-Female Ratio in Autism Spectrum Disorder? A Systematic Review and Meta-Analysis. J Am Acad Child Adolesc Psychiatry. 2017;56:466–474. [PubMed: 28545751]

105. Castro K, Baronio D, Perry IS, Riesgo R dos S, Gottfried C. The effect of ketogenic diet in an animal model of autism induced by prenatal exposure to valproic acid. Nutr Neurosci. 2017;20:343–350. [PubMed: 26856821]

106. IJff DM, Postulart D, Lambrechts DAJE, Majoie MHJM, de Kinderen RJA, Hendriksen JGM, et al. Cognitive and behavioral impact of the ketogenic diet in children and adolescents with refractory epilepsy: A randomized controlled trial. Epilepsy Behav. 2016;60:153–157. [PubMed: 27206235]

107. Ruskin DN, Murphy MI, Slade SL, Masino SA. Ketogenic diet improves behaviors in a maternal immune activation model of autism spectrum disorder. PLOS ONE. 2017;12:e0171643. [PubMed: 28166277]

108. Spilioti M, Evangeliou A, Tramma D, Theodoridou Z, Metaxas S, Michailidi E, et al. Evidence for treatable inborn errors of metabolism in a cohort of 187 Greek patients with autism spectrum disorder (ASD). Front Hum Neurosci. 2013;7:858. [PubMed: 24399946]

109. Cermak SA, Curtin C, Bandini LG. Food selectivity and sensory sensitivity in children with autism spectrum disorders. J Am Diet Assoc. 2010;110:238–246. [PubMed: 20102851]

110. Jaglin M, Rhimi M, Philippe C, Pons N, Bruneau A, Goustard B, et al. Indole, a Signaling Molecule Produced by the Gut Microbiota, Negatively Impacts Emotional Behaviors in Rats. Front Neurosci. 2018;12. [PubMed: 29410610]

111. O'Connor JC, Lawson MA, André C, Moreau M, Lestage J, Castanon N, et al. Lipopolysaccharide-induced depressive-like behavior is mediated by indoleamine 2,3-dioxygenase activation in mice. Mol Psychiatry. 2009;14:511–522. [PubMed: 18195714]

112. Tian P, Wang G, Zhao J, Zhang H, Chen W. Bifidobacterium with the role of 5-hydroxytryptophan synthesis regulation alleviates the symptom of depression and related microbiota dysbiosis. J Nutr Biochem. 2019;66:43–51. [PubMed: 30743155]

113. Wang D, Ho L, Faith J, Ono K, Janle EM, Lachcik PJ, et al. Role of intestinal microbiota in the generation of polyphenol-derived phenolic acid mediated attenuation of Alzheimer's disease β-amyloid oligomerization. Mol Nutr Food Res. 2015;59:1025–1040. [PubMed: 25689033]

114. Reay WR, Cairns MJ. The role of the retinoids in schizophrenia: genomic and clinical perspectives. Mol Psychiatry. 2020;25:706–718. [PubMed: 31666680]

115. Baranova J, Dragunas G, Botellho MCS, Ayub ALP, Bueno-Alves R, Alencar RR, et al. Autism Spectrum Disorder: Signaling Pathways and Prospective Therapeutic Targets. Cell Mol Neurobiol. 2020. 28 May 2020. 10.1007/s10571-020-00882-7.

116. Lai X, Wu X, Hou N, Liu S, Li Q, Yang T, et al. Vitamin A Deficiency Induces Autistic-Like Behaviors in Rats by Regulating the RARβ-CD38-Oxytocin Axis in the Hypothalamus. Mol Nutr Food Res. 2018;62.
117. Bent S, Lawton B, Warren T, Widjaja F, Dang K, Fahey JW, et al. Identification of urinary metabolites that correlate with clinical improvements in children with autism treated with sulforaphane from broccoli. Mol Autism. 2018;9. [PubMed: 29423135]
118. Angelis MD, Piccolo M, Vannini L, Siragusa S, Giacomo AD, Serrazzanetti DI, et al. Fecal Microbiota and Metabolome of Children with Autism and Pervasive Developmental Disorder Not Otherwise Specified. PLOS ONE. 2013;8:e76993. [PubMed: 24130822]
119. Diémé B, Mavel S, Blasco H, Tripi G, Bonnet-Brilhault F, Malvy J, et al. Metabolomics Study of Urine in Autism Spectrum Disorders Using a Multiplatform Analytical Methodology. J Proteome Res. 2015;14:5273–5282. [PubMed: 26538324]
120. Kałużna-Czaplińska J, Żurawicz E, Struck W, Markuszewski M. Identification of organic acids as potential biomarkers in the urine of autistic children using gas chromatography/mass spectrometry. J Chromatogr B Analyt Technol Biomed Life Sci. 2014;966:70–76.
121. Johannsen WJ, Friedman SH, Feldman EI, Negrete A. A Re-examination of the Hippuric Acid--Anxiety Relationship. Psychosom Med. 1962;24:569. [PubMed: 13957814]
122. Needham BD, Adame MD, Serena G, Rose DR, Preston GM, Conrad MC, et al. Plasma and Fecal Metabolite Profiles in Autism Spectrum Disorder. Biol Psychiatry. 2020. 10 October 2020. 10.1016/j.biopsych.2020.09.025.
123. Frye RE, Melnyk S, MacFabe DF. Unique acyl-carnitine profiles are potential biomarkers for acquired mitochondrial disease in autism spectrum disorder. Transl Psychiatry. 2013;3:e220. [PubMed: 23340503]
124. Naviaux RK, Curtis B, Li K, Naviaux JC, Bright AT, Reiner GE, et al. Low-dose suramin in autism spectrum disorder: a small, phase I/II, randomized clinical trial. Ann Clin Transl Neurol. 2017;4:491–505. [PubMed: 28695149]
125. Li Qi, Zhang Chunhua. A metabolome study on 90 autism spectrum disorder patients by mass spectrometry. Med Mass Spectrom. 2017;1.
126. Aydın Hİ, Sönmez FM. A novel mutation in two cousins with guanidinoacetate methyltransferase (GAMT) deficiency presented with autism. Turk J Pediatr. 2019;61:92–96. [PubMed: 31559727]
127. Cameron JM, Levandovskiy V, Roberts W, Anagnostou E, Scherer S, Loh A, et al. Variability of Creatine Metabolism Genes in Children with Autism Spectrum Disorder. Int J Mol Sci. 2017;18. [PubMed: 29267212]
128. Schulze A, Bauman M, Tsai AC-H, Reynolds A, Roberts W, Anagnostou E, et al. Prevalence of Creatine Deficiency Syndromes in Children With Nonsyndromic Autism. Pediatrics. 2016;137. [PubMed: 27543009]
129. Rose S, Niyazov DM, Rossignol DA, Goldenthal M, Kahler SG, Frye RE. Clinical and Molecular Characteristics of Mitochondrial Dysfunction in Autism Spectrum Disorder. Mol Diagn Ther. 2018;22:571–593. [PubMed: 30039193]
130. Sotnikova TD, Beaulieu J-M, Espinoza S, Masri B, Zhang X, Salahpour A, et al. The dopamine metabolite 3-methoxytyramine is a neuromodulator. PloS One. 2010;5:e13452. [PubMed: 20976142]
131. Nakazato T The medial prefrontal cortex mediates 3-methoxytyramine-induced behavioural changes in rat. Eur J Pharmacol. 2002;442:73–79. [PubMed: 12020684]
132. Frye RE. Metabolic and mitochondrial disorders associated with epilepsy in children with autism spectrum disorder. Epilepsy Behav EB. 2015;47:147–157.
133. Needham BD, Adame MD, Serena G, Rose DR, Preston GM, Conrad MC, et al. Plasma and Fecal Metabolite Profiles in Autism Spectrum Disorder. BioRxiv. 2020:2020.05.17.098806.
134. Jin Y, Yan E, Li X, Fan Y, Zhao Y, Liu Z, et al. Neuroprotective effect of sodium ferulate and signal transduction mechanisms in the aged rat hippocampus. Acta Pharmacol Sin. 2008;29:1399–1408. [PubMed: 19026158]
135. Aabed K, Bhat RS, Al-Dbass A, Moubayed N, Algahtani N, Merghani NM, et al. Bee pollen and propolis improve neuroinflammation and dysbiosis induced by propionic acid, a short chain fatty acid in a rodent model of autism. Lipids Health Dis. 2019;18:200. [PubMed: 31733650]

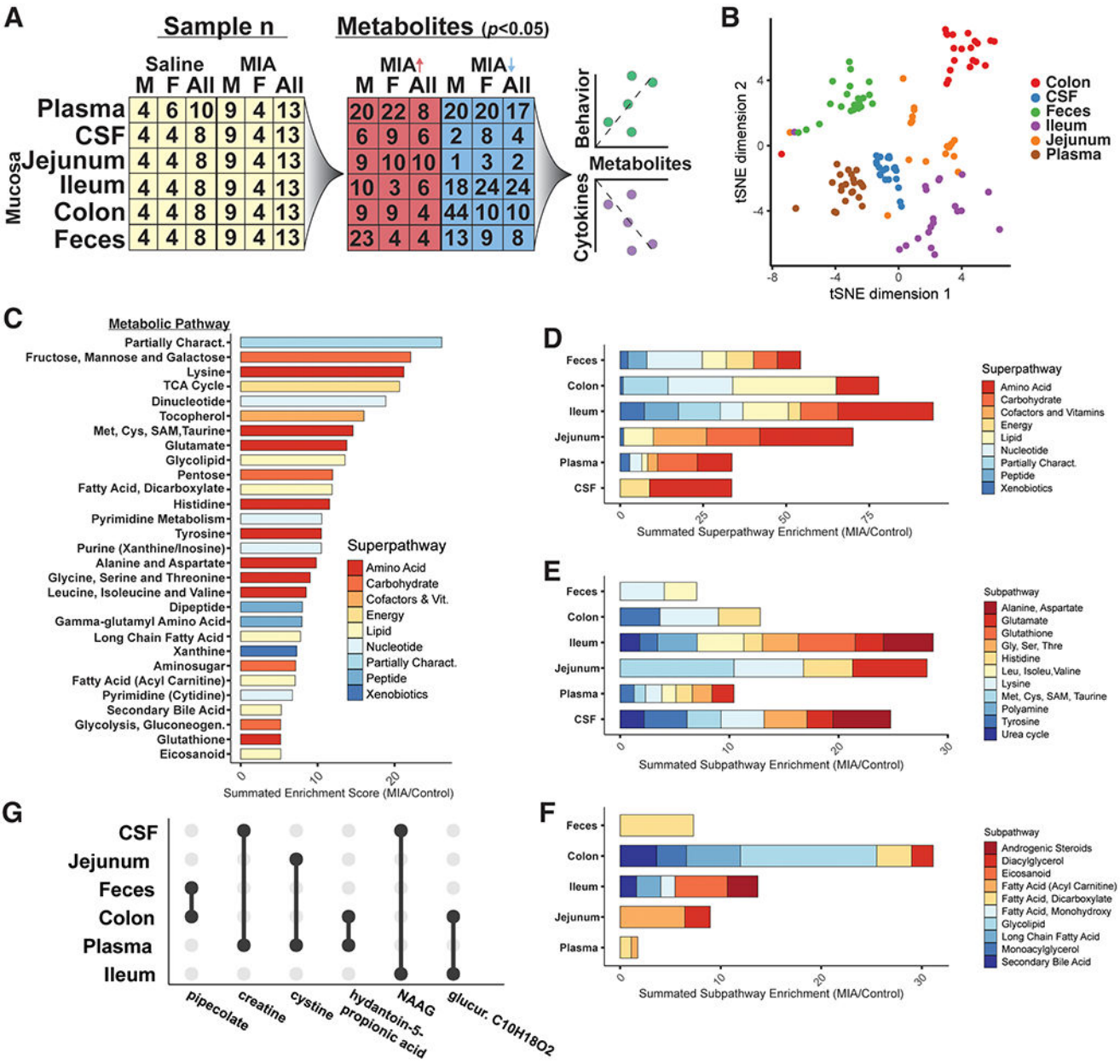

Figure 1. Metabolic profiles differ between MIA and control offspring in NHPs, especially in amino acid and lipid metabolic pathways.

(a) Schematic of the study showing in yellow the sample types and number of male (M), female (F), and total (All) samples from control or MIA offspring. The number of significantly different ($p \leq 0.05$) metabolites between the two treatment groups are shown in red (elevated in MIA offspring) and blue (decreased in MIA offspring). Metabolites with differential levels between groups were then evaluated for correlations with either cytokine levels in blood and brain and gastrointestinal tissue or behavior scores of the animals. (b) tSNE analysis demonstrating the clustering of samples according to tissue type. Each data point represents a sample from an individual animal, with sample type colored according to the legend. (c) Overview level pathway enrichment analysis with all samples and tissue

types combined. Metabolic pathways are listed along the y-axis and enrichment scores (with a cutoff of 5) along the x-axis, colored by superpathway group listed in legend. (d-f) Pathway enrichment summaries are provided, stratified by sample type and juxtaposed for comparison across tissues for superpathway (d), amino acid metabolic subpathways (e), and lipid metabolic subpathways (f). (g) Upset plot displaying metabolites with an association with treatment in multiple tissues. Solid points indicate a significant association ($p \leq 0.05$)

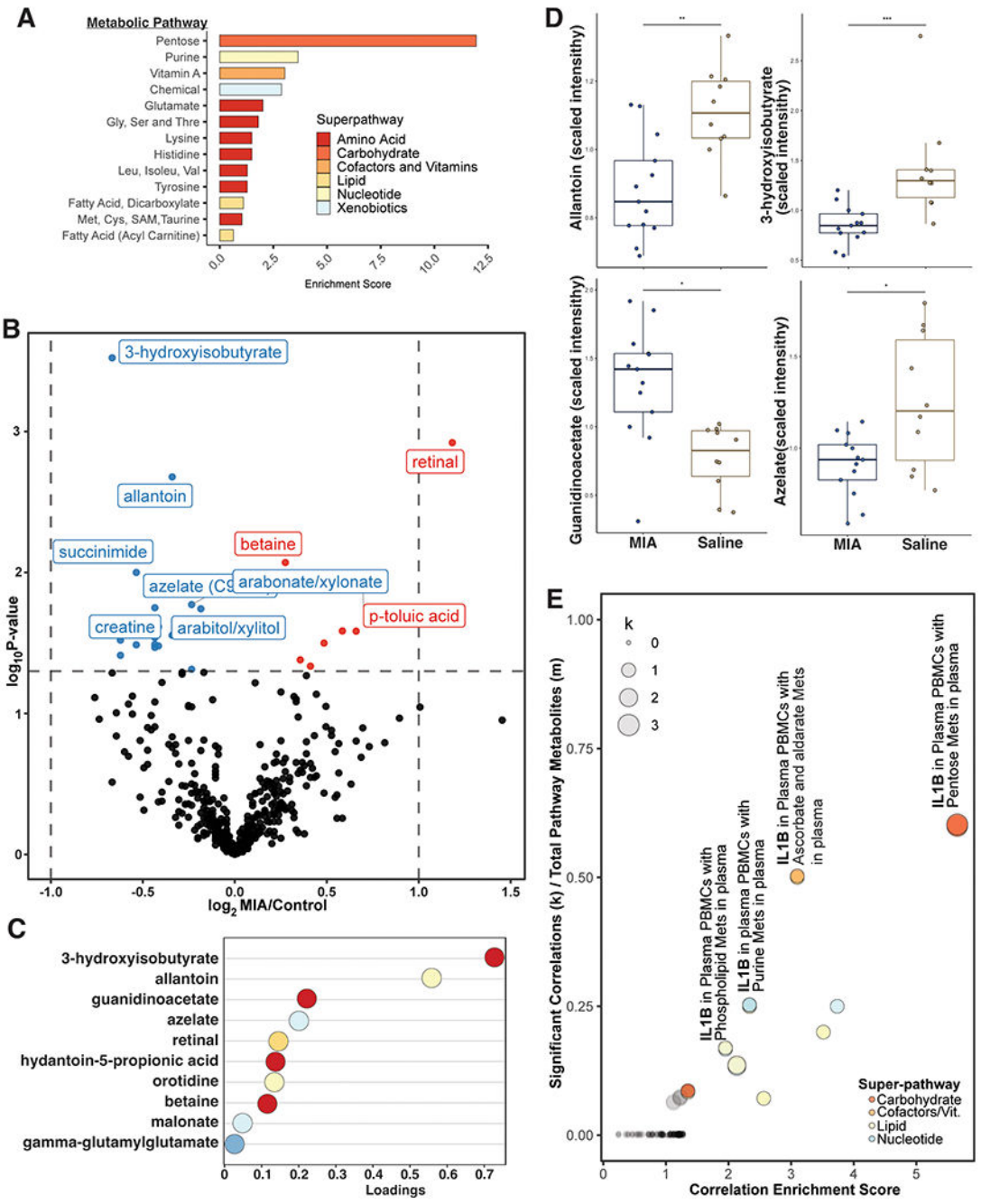

Figure 2. Characteristic differences between MIA and control offspring in plasma samples.

(a) Pathway enrichment analysis comparing all MIA to control plasma samples. Metabolic pathways are listed along the y-axis and enrichment score along the x-axis, colored by superpathway group listed in legend. (b) Volcano plot of plasma metabolite levels, with $\log_2$ fold change (MIA/control) along x-axis and −log10 *p*-value along the y-axis. (c) Top ten most discriminatory metabolites driving the separation of groups by sPLS-DA for the first component. (d) Box plots showing individual scaled intensity levels of allantoin, 3-hydroxyisobutyrate, guanidinoacetate, and azelate, four highly discriminatory plasma

metabolites. (e) Bubble plot displaying enrichment scores of subpathways calculated for plasma metabolite correlations to tissue specific cytokines. Size of each data point portrays the number of significant correlations within a subpathway (k) and the y-axis shows the ratio of (k) to the total number of metabolites within the subpathway. * $p \leq 0.05$; ** $p \leq 0.01$; *** $p \leq 0.01$.

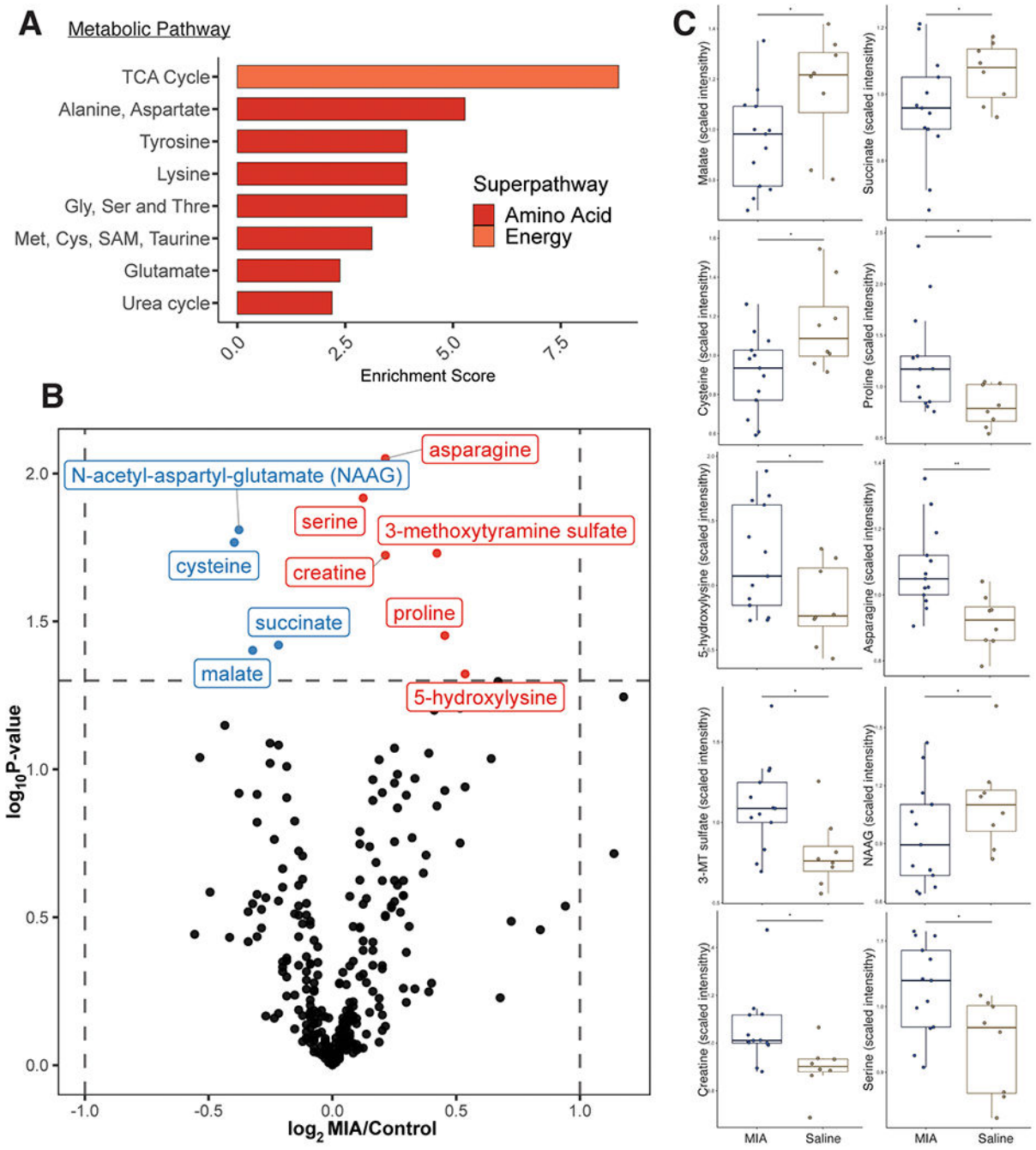

Figure 3. Characteristic differences between MIA and control offspring in CSF samples.

(a) Pathway enrichment analysis comparing all MIA to control CSF samples. Metabolic pathways are listed along the y-axis and enrichment score along the x-axis, colored by superpathway group listed in legend. (b) Volcano plot of CSF metabolite levels, showing $\log_2$ fold change (MIA/control) along x-axis and −log10 *p*-value along the y-axis. (c) Box plots showing individual scaled intensity levels of malate, succinate, cysteine, asparagine, 3-methoxytyramine (3-MT) sulfate, N-acetylaspartylglutamate (NAAG), creatine, and serine. * $p \leq 0.05$; ** $p \leq 0.01$.

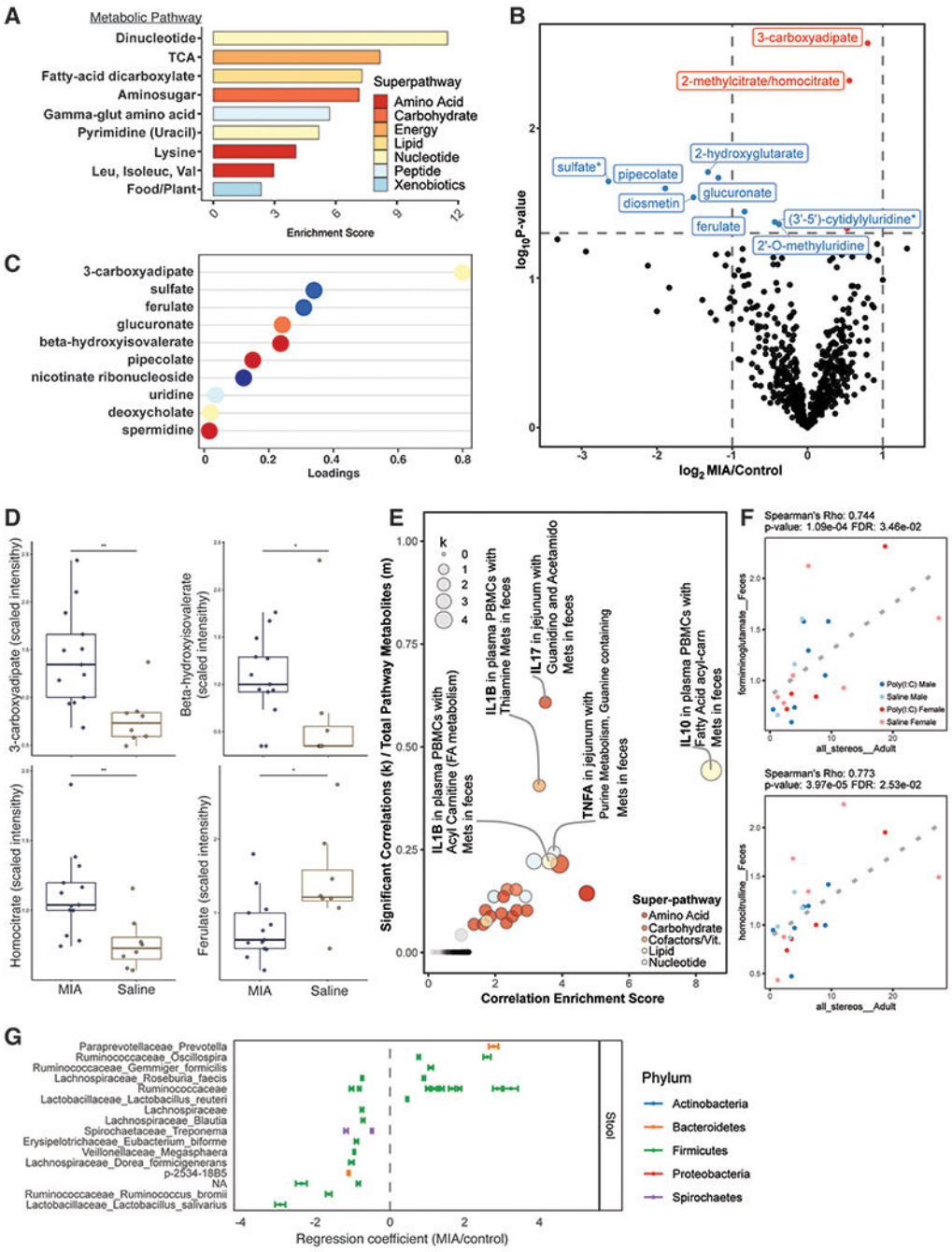

Figure 4. Characteristic differences between MIA and control offspring in fecal samples.

(a) Pathway enrichment analysis comparing all MIA to control fecal samples. Metabolic pathways are listed along the y-axis and enrichment score along the x-axis, colored by superpathway group listed in legend. (b) Volcano plot fecal metabolite levels, with $\log_2$ fold change (MIA/control) along x-axis and −log10 *p*-value along the y-axis. (c) Top ten most discriminatory fecal metabolites driving the separation of groups by sPLS-DA for the first component. (d) Box plots showing individual scaled intensity levels of 3-carboxyadipate, beta-hydroxyisobutyrate, homocitrate, and ferulate, four highly discriminatory fecal

metabolites. (e) Bubble plot displaying enrichment scores of subpathways calculated for fecal metabolite correlations to tissue specific cytokines. Size of each data point portrays the number of significant correlations within a subpathway (k) and the y-axis shows the ratio of (k) to the total number of metabolites within the subpathway (f) Scatterplots displaying linear regression of fecal formiminoglutamate (top) and homocitruline (bottom) levels and adult stereotypic behaviors of NHPs. (g) Regression coefficients for the top 30 most significant ($q \leq 0.1$) ASVs for treatment status. ASVs are labeled as their taxonomic classification at the Family through Species level and colored by Phylum. * $p \leq 0.05$; ** $p \leq 0.01$.

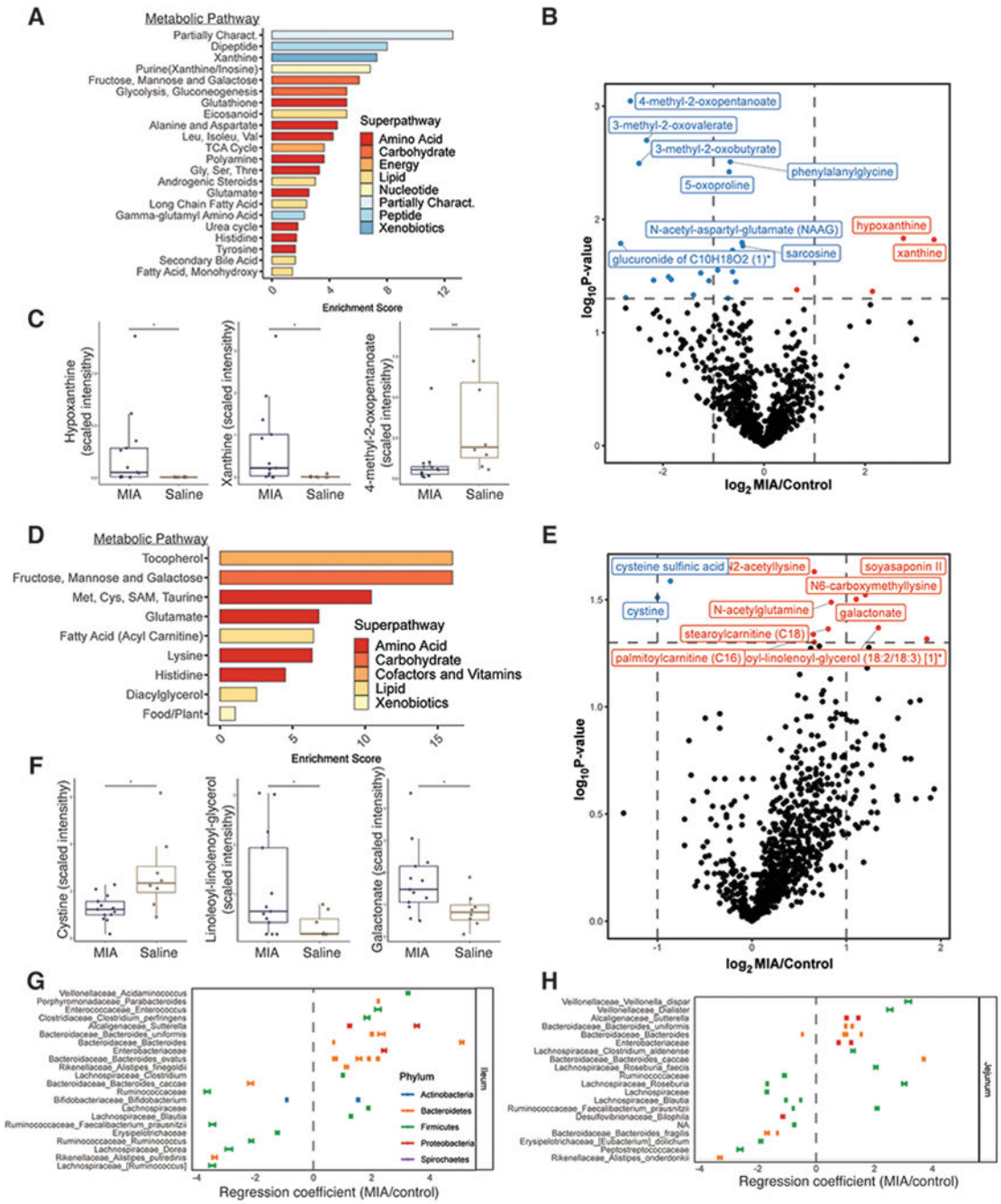

Figure 5. Characteristic differences between MIA and control offspring in intestinal scraping samples from the ileum and jejunum.

(a) Pathway enrichment analysis comparing all MIA to control ileum scrapings samples. Metabolic pathways are listed along the y-axis and enrichment score along the x-axis, colored by superpathway group listed in legend. (b) Volcano plot of ileum scrapings showing $\log_2$ fold change (MIA/control) along x-axis and −log10 *p*-value along the y-axis. (c) Box plots showing individual scaled intensity levels of cystine, linoleoyl-linolenoyl-glycerol, and galactonate in ileum samples. (d) Pathway enrichment analysis comparing all MIA to control jejunum scrapings samples. Metabolic pathways are listed along the y-axis

and enrichment score along the x-axis, colored by superpathway group listed in legend. (e) Volcano plot of jejunum scrapings showing $\log_2$ fold change (MIA/control) along x-axis and −log10 *p*-value along the y-axis. (f) Box plots showing individual scaled intensity levels of hypoxanthine, xanthine, and 4-methyl-2-oxopentanoate in jejunum samples. (g, h) Regression coefficients for the top 30 most significant (q ≤ 0.1) ASVs for treatment status in the ileum (g), and jejunum (h). ASVs are labeled as their taxonomic classification at the Family through Species level and colored by Phylum. * $p \leq 0.05$; ** $p \leq 0.01$; *** $p \leq 0.01$, **** $p \leq 0.001$.

Table 1.

Key differential metabolites and known ASD contexts.

	Key metabolites	Associations with preclinical/clinical ASD
Plasma	Retinal elevated	Important for multiple neurodevelopmental processes and linked to ASD and schizophrenia[114–116]
	Phenolic metabolites correlated with each other	Phenolic metabolites previously implicated in human ASD metabolomics studies[10, 42, 43, 46, 49, 51–55, 68, 70, 117–122]
	Acyl-carnitines correlated with each other	Can be readouts of mitochondrial function and may be relevant biomarkers in ASD[59, 123]
	Allantoin lower	Lower levels of allantoin have previously been observed in MIA mice and then restored along with normal behavior after antipurinergic therapy[70]. This same treatment resulted in improved behavioral metrics in a small clinical trial[124].
	3-hydroxyisobutyrate lower	Lower trend previously observed in plasma and urine samples from children with ASD[47, 125].
	Guanidinoacetate elevated/ Creatine lower	Guanidinoacetate is converted to creatine by the enzyme guanidinoacetate methyltransferase (GAMT), which is a known risk allele for ASD[126–128]. Interestingly, we observe elevated guanidinoacetate (Fig. 2D) and decreased creatine levels (Fig. S3C), and symptoms of severe creatine deficiency overlap with the behavioral features of ASD[127].
	Azelate lower	No known associations with ASD.
CSF	Asparagine elevated, Cysteine lower, other TCA-related metabolites at altered levels	Energy metabolites have been previously associated with ASD[129].
	3-methoxytyramine (3-MT) elevated	Has been shown to impact stereotypic behavior in rodents[130, 131].
Feces	3-carboxyadipate elevated	No known associations with ASD.
	Beta-hydroxyisovalerate elevated	Excretion of beta-hydroxyisovalerate is an indicator of biotin disorders, which have been associated with ASD in humans[132].
	Homocitrate elevated	No known associations with ASD.
	Ferulate lower	Ferulate, which is lower in MIA fecal samples, and its downstream bacterial metabolite dihydroferulic acid, which is decreased in female MIA samples (Supplementary Table S5), possess anti-inflammatory properties, have been found to be lower in feces of ASD children[133], and have been explored as part of a complex mixture of a therapeutic for the propionic acid-induced ASD rodent model[134, 135].
	Purine and pyrimidine nucleotide metabolite levels correlated with each other	Alterations to nucleotide metabolism have commonly been observed in ASD[93, 94], and purinergic treatments have shown promise in MIA mice[70, 92].
Scrapings	Xanthine elevated (ileum)	Alterations to nucleotide metabolism have commonly been observed in ASD[93, 94], and purinergic treatments have shown promise in MIA mice[70, 92].
	Hypoxanthine elevated (ileum)	Alterations to nucleotide metabolism have commonly been observed in ASD[93, 94], and purinergic treatments have shown promise in MIA mice[70, 92].
	Gentisate lower (colon)	Gentisate is a key phenolic intermediate in microbial degradation of polycyclic aromatic hydrocarbons and has been found to be decreased in the feces of ASD children[133].